Journal of Materials Chemistry C

Accepted Manuscript

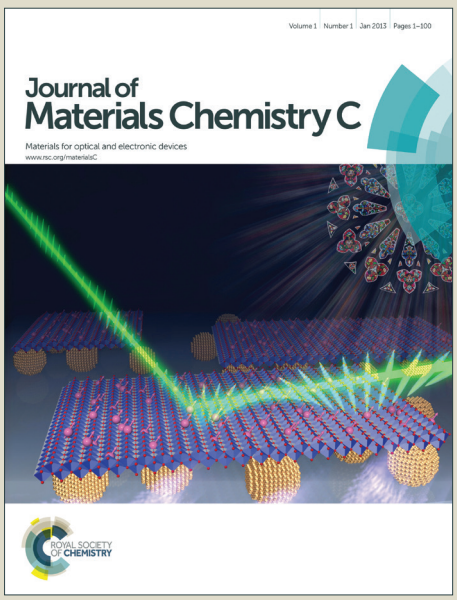

ROYAL SOCIETY OF CHEMISTRY

www.rsc.org/materialsC

Journal Name

RSCPublishing

ARTICLE

Functionalized Salen ligands linking with non-conjugated bridges: unique and colorful aggregation-induced emission, mechanism, and applications†

Cite this: DOI: 10.1039/x0xx00000x

Received 00th January 2012,
Accepted 00th January 2012

DOI: 10.1039/x0xx00000x

www.rsc.org/

Jinghui Cheng,‡[a] Yuanxi Li,‡[b] Rui Sun,[a] Jiaoyan Liu,[a] Fei Gou,[a] Xiangge Zhou,[a] Haifeng Xiang,*[a] and Jin Liu*[b]

A series of novel, simple, and colorful Salen ligands (56 samples), salicylaldehyde-based *bis*-Schiff bases, linking with different non-conjugated alkyl bridges ($(CH_2)_n$, n = 2–9, 12; cyclohexyl) and containing different electron-accepting (–NO_2, –F, and –Cl), electron-donating (–OMe, –OH, and –NEt_2), or steric hindrance (–*t*-butyl) substituents or π-extended system (naphthalene ring) have been designed and synthesized. The photophysical properties of these Salen ligands can be well-tuned by the introduction of side functional substituents, π-extended system, and central *N*-alkyl chain bridges. It is unusual that they contain a small π-conjugated system but display strong blue, green, and red aggregation-induced emission (AIE) with large Stokes shifts (up to 162 nm) and high fluorescence quantum yields (up to 0.44 and 0.75 in water and solid, respectively). Combining with their advantages of AIE and good stability and biocompatibility, the Salen ligands can be potentially used in mechanofluorochromism (crystal-defect-induced emission) and living cell imaging. Moreover, the inherent relationships between their chemical structures and AIE properties are studied, which provide unequivocal insights for the design of AIE-active dyes.

Introduction

The design and synthesis of organic luminescent (fluorescent or phosphorescent) materials[1] have attracted great interests in a variety of scientific communities due to their wide and useful applications, such as organic light-emitting diodes (OLEDs),[2] light-emitting electrochemical cells (LECs),[3] triplet–triplet annihilation based upconversion,[4] fluorescence probes,[5] therapy,[6] and bio-imaging.[7] In general, a typical organic luminescent material is a polycyclic aromatic molecule with one plane of big π-conjugated system, which would be favorable to the larger wavelength of absorption (λ_{abs}) and emission (λ_{em}) bands with the stronger absorption intensity and higher luminescence quantum yield (Φ). However, it is notorious that luminescence is often weakened or quenched at high concentrations or in solid state, due to the aggregation-caused quenching (ACQ) effect[8] that is usually arisen from the intermolecular π–π stacking interactions of π-conjugated plane molecules. In fact, the ACQ effect is usually harmful for some practical applications. In the case of sensing applications, the preferred work conditions are aqueous media, but it is incongruous that most of organic luminescent probes containing hydrophobic polycyclic aromatics have a poor solubility in water, which might cause aggregation in water and subsequently lead to luminescence quenching by the ACQ effect. Moreover, the ACQ effect is more harmful and challenging for OLED and LEC applications, where the luminophores are in solid state and might have a more severe ACQ effect. Tang et. al. recently discovered an exactly opposite phenomenon of aggregation-induced emission (AIE).[9] Since then AIE-active materials have been becoming one of the most active and hottest research areas in material field.[10]

N,N′-Bis(salicylidene)ethylenediamine (Salen), a particular class of tetradentate chelating *bis*-Schiff base (Fig. 1), can be synthesized by the condensation of diamine with 2 equivalents of salicylaldehyde. Because of their facile preparation, good stabilities, biological activities, and rich photophysical properties, Salen ligands and their associated metal complexes have attracted much attention in many fields, including catalysts,[11] DNA cleavage,[12] optical and magnetic materials,[13] supramolecular materials,[14] cell imaging,[15] and OLEDs.[16] Our research work is focusing on the synthesis, photophysical properties, and sensing applications of Salen ligands.[17] Like a typical organic luminescent material, most of these Salen ligands containing one big plane of π-conjugated system usually exhibit much stronger fluorescence in dilute organic solution than in solid state or water, indicating the possible existence of ACQ. For example, one maleonitrile-based Salen ligand (CN) (Fig. 1) has one big plane of π-conjugated system, resulting in the strong fluorescence with an unexpectedly high quantum yield of 0.80 in dilute MeCN but no fluorescence in water or solid state.[17c]

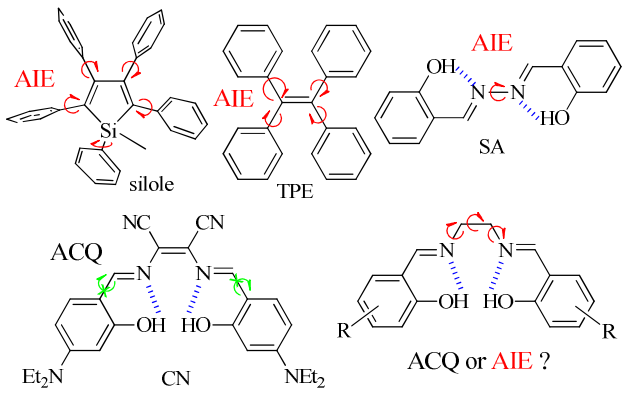

Fig. 1 Chemical structures of AIE-active silole, TPE, and SA and ACQ-active Salen ligand of CN.

Up to now, most of AIE-active materials have non-plane AIE cores, such as silole[10,18] or tetraphenylethene (TPE) (Fig. 1),[9,19] In dilute organic solution, their phenyl groups rotor undergo dynamic intramolecular rotations (IRs), which provide a possible way to non-radiatively annihilate its excited states and result in the absence of luminescence. In the aggregates, however, these IRs are greatly restricted owing to the physical constraint. In addition, these non-plane molecules with propeller shape cannot be packed through intermolecular face-to-face π–π interactions (Fig. 1). This restriction of both IRs and π–π interactions blocks the non-radiative pathway and opens up the radiative channel. On the other hand, the previous works of our group and other groups revealed that salicylaldehyde azine (SA) (Fig. 1) molecules exhibit the nature of AIE,[20] even though they have a plane structure and similar synthetic process with Salen ligands. Unlike TPE and silole, the IRs of SA are rotatable N–N single bonds rather than C–C single bonds, because the existence of intramolecular hydrogen bonds restricts the rotations of C–C single bonds (Fig. 1). Plane SA molecules are cross stacking with a short interplanar distance (*d*) of ~3.45 Å and weak intermolecular face-to-face π–π interactions, which ensures to eliminate the rotations of N–N single bonds and results in AIE thereby.[20d] Moreover, the recent works also demonstrated that the presence of side alkyl chains at the AIE-active core would affect the mechanochromic properties.[21] Is it possible to achieve and improve AIE properties of Salen ligands if more rotations of C–C single bonds (alkyl chains) are introduced to act as the central linker (Fig. 1)? To the best of our knowledge, however, in the literature there is still a scarcity of reports on such AIE-active materials, because they linking with non-conjugated alkyl bridges have a very small π-conjugated system and are taken for granted as non-emissive materials hereby. Especially, the effects of the length of the central alkyl chain on AIE properties have been still unclear yet. The detailed study on the central alkyl bridges in cooperation with other side functional substituents should be required to clarify the intrinsic AIE properties. Herein, we report the unique AIE properties, mechanofluorochromism, and cell imaging of Salen ligands (56 samples), which contain different non-conjugated alkyl bridges ($(CH_2)_n$, n = 2–9, 12; cyclohexyl) and different electron-accepting ($–NO_2$, –F, and –Cl), electron-donating (–OMe, –OH, and $–NEt_2$), or steric hindrance (–*t*-butyl) substituents or π-extended system (naphthalene ring). Although these Salen ligands have a small π-conjugated system, they display strong blue, green, and red AIE with large Stokes shifts (up to 162 nm) and high fluorescence quantum yields up to 0.44 and 0.75 in water and solid, respectively.

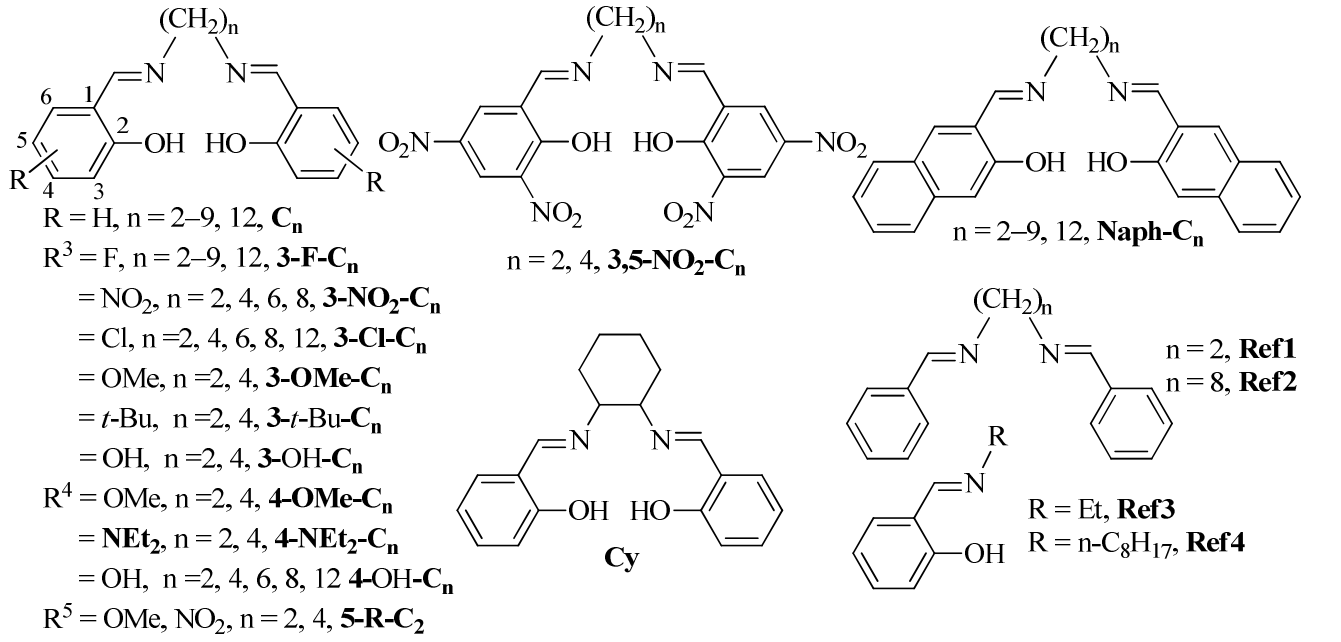

Fig. 2 Chemical structure of organic dyes studied in this work.

Journal Name

RSCPublishing

ARTICLE

Results and discussion

Synthesis and characterization

Compared with other well-known robust and expensive tetradentate porphyrin ligands,[22] inexpensive Salen ligands are facile to prepare and tune fluorescence bands.[17c] The general method of preparation of Schiff bases is quite straightforward and consists of the condensation reaction of primary diamines with an aldehyde precursor usually in alcoholic solution or toluene and sometimes under reflux conditions. The reaction is acid catalyzed but catalysts are not generally required when aliphatic amines are involved. In order to achieve high yield, the water produced in the reversible reaction can be removed by azeotropic distillation, when conducting the synthesis in toluene solution. Finally, the condensation of primary diamine with 2 equivalents of salicylaldehyde precursor in ethanol under refluxing condition was adopted for the preparation of Salen ligands in this work. Most of Salen ligands have a good solubility in organic solvent, such as CH_2Cl_2, CH_3CN, EtOH, and DMF, and bad solubility in hexane and petroleum ether, especially bad solubility in water. Usually, in order to avoid the degradation of Schiff bases during the purification step through hydrolysis, it is better to purify Schiff bases by re-crystallization (e.g. CH_2Cl_2/hexane) rather than running chromatography even though most of Salen ligands are stable enough for running chromatography. Most of Salen ligands can grow good-quality single crystals by the method of slow solvent diffusion/evaporation (CH_2Cl_2/hexane). Unlike many free Schiff bases that are not always stable in solution and need to prepare by template synthesis in the presence of a metal ion, all Salen ligands either in solution or in solid state are stable within several months under air. For the purpose of the mechanism evaluation, the reference substances, *N,N′*-dibenzylideneethane-1,2-diamine (**Ref1**), *N,N′*-dibenzylideneethane-1,8-diamine (**Ref2**), 2-((ethylimino)methyl)phenol (**Ref3**), and (E)-2-((octylimino)methyl)phenol (**Ref4**) (Fig. 2) were prepared as well.

Photophysical and AIE properties

The room-temperature optical properties of the synthesized Salen ligands were investigated by UV/visible absorption and fluorescence emission spectra and are listed in Table 1. As examples, the absorption spectra of $\mathbf{C_2}$–$\mathbf{C_9}$, $\mathbf{C_{12}}$ and **Cy** in pure organic solvent of CH_2Cl_2 (1×10^{-5} mol dm^{-3}) are given in Fig. 3a. They containing the same phenol and different alkyl bridge have similar absorption intensity and bands (λ_{abs}: 314–318 nm), indicating that the non-conjugated alkyl bridges have little effect on their absorption. The lower energy absorption band of $\mathbf{C_4}$ (λ_{abs} = 316 nm) is reproduced well using gas-phase time-dependent-DFT (TD-DFT) calculations, which predict one absorption maximum at 311 nm (Fig. S1 in Supporting information). The lower energy absorption ($S_0 \rightarrow S_1$) mainly corresponds to the highest occupied molecular orbital (HOMO) $\rightarrow$ lowest unoccupied molecular orbital (LUMO) and HOMO−1 $\rightarrow$ LUMO+1. The energy level diagram of $\mathbf{C_4}$ with orbital isosurfaces is also given in Fig. S2. Based on these frontier molecular orbitals and absorption spectra, the lower energy absorption can mainly be assigned to the $\pi \rightarrow \pi^*$ transition involving molecular orbitals essentially localized on the C=N group and the phenol ring[17a,c] but little contribution from non-conjugated alkyl bridges. Moreover, the presence of steric hindrance –*t*-butyl (**3-*t*-Bu-$\mathbf{C_2}$**, λ_{abs} = 323 nm), weak electron-accepting –F (**3-F-$\mathbf{C_2}$**, λ_{abs} = 316 nm), or –Cl (**3-Cl-$\mathbf{C_2}$**, λ_{abs} = 322 nm) substituents at $\mathbf{C_2}$ (λ_{abs} = 318 nm) have little effect on absorption spectra. However, if π-extended system (**Naph-$\mathbf{C_2}$**, λ_{abs} = 420 nm), strong electron-donating –OMe (**3-OMe-$\mathbf{C_2}$**, λ_{abs} = 332 nm; **4-OMe-$\mathbf{C_2}$**, λ_{abs} = 392 nm; **5-OMe-$\mathbf{C_2}$**, λ_{abs} = 346 nm), –NEt_2 (**4-$\mathbf{NEt_2}$-$\mathbf{C_2}$**, λ_{abs} = 336 nm), or strong electron-accepting –NO_2 (**3-$\mathbf{NO_2}$-$\mathbf{C_2}$**, λ_{abs} = 442 nm; **3,5-$\mathbf{NO_2}$-$\mathbf{C_2}$**, λ_{abs} = 378 nm) substituents are introduced, obvious red shifts in absorption spectra would be observed (Fig. 3b and Table 1).

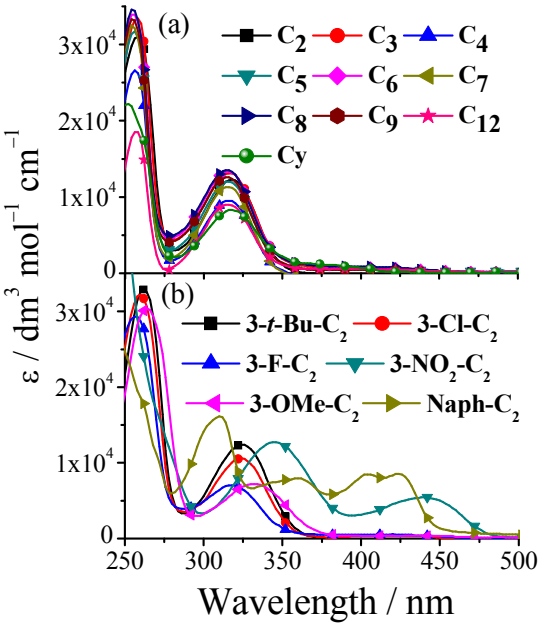

Fig. 3 Absorption spectra of some selected Salen ligands in CH_2Cl_2.

As expected, most of the Salen ligands have weak fluorescence in pure organic solvent of CH_2Cl_2 or MeCN (Table 1). For example, the emission spectra of **C_2** are depicted in Fig. 4. In the dilute organic solution of MeCN, the IRs of central ethane bridge in **C_2** provide a possible way to non-radiatively annihilate its excited states, resulting in the absence of luminescence. Nonetheless, when water is added into MeCN, its emission is enhanced due to the formation of aggregation. This aggregation is further confirmed by the fact of its red-shifted absorption spectra (Fig. S3). When the volume fraction (*f*) of water is increased to 94 %, its emission attains the maximum (Φ = 0.025) with a large Stokes shift of 119 nm. Moreover, **C_2** in solid state emits strong blue-green emission (Φ = 0.030) under 360 nm UV lamp (Fig. 5). All the aforementioned findings confirm the fact of its AIE nature.

Table 1 Photophysical data of the Salen ligands and complexes at room temperature. Sample without solid-state emission data is nonemissive in solid state.

Salen ligand	medium	λ_{abs} /nm (ε /dm^3 mol^{-1} cm^{-1})	λ_{em} /nm	Stokes shift /nm	Φ	*f* /%
C_2	CH_2Cl_2	258(3.1×10^4); 318(1.23×10^4)	369		0.0072	
	Water	314; 378	497	119	0.025	94
	Solid		500		0.030	
3-NO_2-C_2	CH_2Cl_2	344(1.2×10^4); 442(4.7×10^3)	500		0.071	
	Water	430	577	137	0.036	98
	Solid		588		0.037	
3,5-NO_2-C_2	CH_2Cl_2	378(6.3×10^3)	441		0.026	
3-F-C_2	CH_2Cl_2	256(2.93×10^4); 316(7.0×10^3); 404(5.0×10^2)	440		0.003	
	Water	318; 380	504	124	0.24	80
	Solid		507		0.38	
3-Cl-C_2	CH_2Cl_2	260(3.22×10^4); 322(1.05×10^4); 422(2.0×10^2)	370		0.0092	
	Water	318; 388	500	112	0.11	96
	Solid		555		0.12	
4-NEt_2-C_2	CH_2Cl_2	342(7.88×10^4)	432		0.070	
Naph-C_2	CH_2Cl_2	306(1.62×10^4); 364(8.3×10^3); 420(8.9×10^3); 424(8.8×10^3)	466		0.092	
	Solid		473		0.086	
3-OMe-C_2	CH_2Cl_2	264(3.04×10^4); 332(7.2×10^3)	369		0.065	
4-OMe-C_2	CH_2Cl_2	276(3.73×10^4); 308(2.63×10^4); 392(2.3×10^3)	368		0.063	
5-OMe-C_2	CH_2Cl_2	260(1.35×10^4); 346(8.6×10^3)	369		0.044	
3-tBu-C_2	CH_2Cl_2	262(3.29×10^4); 324(1.24×10^4)	369		0.0076	
4-OH-C_2	CH_2Cl_2	275(6.1×10^4); 310(4.55×10^4); 385(2.1×10^3)	408		0.0027	
	Solid		539		0.09	
3-OH-C_2	CH_2Cl_2	310(3.3×10^4); 350(2.0×10^3); 430(3.3×10^4)	406		0.0013	
	Solid		552		0.011	
C_3	CH_2Cl_2	256(3.32×10^4); 316(1.31×10^4)	369		0.0066	
3-F-C_3	CH_2Cl_2	258(3.75×10^4); 320(8.3×10^3); 408(1.0×10^3)	445		0.0030	
	Water	268; 380	504	124	0.12	80
	Solid		513		0.13	
Naph-C_3	CH_2Cl_2	308(1.29×10^4); 360(5.6×10^3); 402((7.6×10^3); 4204(7.7×10^3)	458		0.077	
	Solid		478		0.080	
C_4	CH_2Cl_2	254(2.61×10^4); 316(9.5×10^3)	369		0.011	
	Water	314; 382	499	117	0.13	92
	Solid		500		0.19	
3-NO_2-C_4	CH_2Cl_2	346(7.3×10^3); 438(9.6×10^3)	499		0.0065	
	Solid		558		0.082	
5-NO_2-C_4	CH_2Cl_2	348(3.3×10^4); 404(3.46×10^4)	490		0.0055	
	Solid		556		0.052	
3,5-NO_2-C_4	CH_2Cl_2	396(1.8×10^3)	560		0.020	
3-F-C_4	CH_2Cl_2	256(2.95×10^4); 312(8.6×10^3); 410(2.6×10^3)	364		0.0039	
	Water	314; 380	499	119	0.11	98
	Solid		508		0.19	
3-Cl-C_4	CH_2Cl_2	254(1.39×10^4); 320(3.7×10^3); 410(8.0×10^2)	434		0.0094	
	Water	276; 392	501	109	0.17	70

	Solid		524		0.11	
3-OMe-C_4	CH_2Cl_2	264(2.77×10^4); 326(6.2×10^3) ; 420(6.0×10^2)	356		0.0038	
	Water	288; 408	536	128	0.091	90
	Solid		542		0.11	
4-OMe-C_4	CH_2Cl_2	276(8.79×10^4); 302(6.06×10^4) ; 388(8.1×10^3)	425		0.0035	
	Water	292; 370	470	100	0.11	92
	Solid		471		0.12	
5-OMe-C_4	CH_2Cl_2	230(1.06×10^5); 258(3.91×10^4) ; 342(2.45×10^4)	410		0.0034	
	Water	334; 426	514	88	0.14	94
	Solid		521		0.17	
4-Net_2-C_4	CH_2Cl_2	336(5.91×10^4)	488		0.097	
Naph-C_4	CH_2Cl_2	308(3.22×10^4); 362(1.18×10^3); 402(2.13×10^3); 422(2.18×10^3)	457		0.089	
	Solid		489		0.091	
3-tBu-C_4	CH_2Cl_2	262(6.55×10^4); 324(2.44×10^4)	410		0.0066	
4-OH-C_4	CH_2Cl_2	275(7.22×10^4); 305(5.15×10^4); 385(4.1×10^3)	409		0.0024	
	Solid		491		0.097	
3-OH-C_4	CH_2Cl_2	315(1.7×10^4); 345(1.7×10^4); 430(2.2×10^4)	404		0.0017	
	Solid		553		0.025	
C_5	CH_2Cl_2	254(3.14×10^4); 314(1.2×10^4)	369		0.0086	
	Water	314; 386	496	110	0.076	
	Solid		498		0.073	
3-F-C_5	CH_2Cl_2	254(3.38×10^4); 316(7.7×10^3); 412(1.9×10^3)	445		0.0027	
	Water	270; 386	500	114	0.14	50
	Solid		504		0.18	
Naph-C_5	CH_2Cl_2	306(2.49×10^4); 362(8.6×10^3); 402(1.78×10^3); 422(1.82×10^3)	457		0.038	
	Solid		489		0.051	
C_6	CH_2Cl_2	256(3.39×10^4); 316(1.33×10^4)	369		0.0069	
	Water	314; 384	496	112	0.095	80
	Solid		495		0.11	
3-F-C_6	CH_2Cl_2	254(3.37×10^4); 320(7.1×10^3); 410(1.8×10^3)	445		0.0053	
	Water	272; 388	498	110	0.12	70
	Solid		506		0.41	
3-Cl-C_6	CH_2Cl_2	258(2.97×10^4); 320(9.6×10^3); 416(2.7×10^3)	446		0.0083	
	Water	274; 394	503	109	0.34	80
	Solid		522		0.36	
3-NO_2-C_6	CH_2Cl_2	350(7.6×10^3); 442(1.87×10^4)	498		0.0047	
	Solid		542		0.034	
Naph-C_6	CH_2Cl_2	308(2.58×10^4); 360(8.6×10^3); 402(1.87×10^3); 422(1.9×10^3)	457		0.078	
	Solid		476		0.086	
4-OH-C_6	CH_2Cl_2	275(5.68×10^4); 305(4.13×10^4); 385(4.5×10^3)	409		0.0023	
C_7	CH_2Cl_2	256(3.21×10^4); 314(1.13×10^4)	357		0.006	
3-F-C_7	CH_2Cl_2	254(3.48×10^4); 316(7.2×10^3); 410(1.8×10^3)	443		0.0012	
	Water	268; 380	501	121	0.11	70
	Solid		518		0.11	
Naph-C_7	CH_2Cl_2	306(2.42×10^4); 358(7.9×10^3); 402(1.82×10^3); 422(1.84×10^3)	457		0.069	
	Solid		483		0.067	
C_8	CH_2Cl_2	254(3.46×10^4); 316(1.35×10^4)	364		0.0092	
	Water	314; 378	497	118	0.093	98
	Solid		498		0.16	
3-NO_2-C_8	CH_2Cl_2	344(8.5×10^3); 440(2.03×10^4)	498		0.0039	
	Water	428	550	122	0.18	98
	Solid		563		0.17	
3-F-C_8	CH_2Cl_2	252(2.98×10^4); 316(6.4×10^3); 410(1.6×10^3)	445		0.005	
	Water	268; 384	498	114	0.12	70
	Solid		509		0.12	
3-Cl-C_8	CH_2Cl_2	256(3.14×10^4); 320(9.6×10^3); 418(3.4×10^3)	484		0.0026	

	Water	314; 388	500	112	0.12	98
	Solid		523		0.11	
Naph-C_8	CH_2Cl_2	306(2.45×10^4); 362(7.9×10^3); 402(1.87×10^3); 422(1.91×10^3)	457		0.045	
	Solid		483		0.049	
4-OH-C_8	CH_2Cl_2	275(4.71×10^4); 305(3.58×10^4); 385(4.9×10^3)	403		0.0021	
C_9	CH_2Cl_2	256(3.31×10^4); 316(1.26×10^4)	365		0.0066	
	Water	312; 398	498	100	0.12	98
	Solid		500		0.17	
3-F-C_9	CH_2Cl_2	254(2.45×10^4); 320(5.4×10^3); 414(1.5×10^3)	445		0.0011	
	Water	268; 378	499	121	0.13	80
	Solid		508		0.11	
Naph-C_9	CH_2Cl_2	306(2.59×10^4); 362(8.6×10^3); 402(1.97×10^3); 422(1.99×10^3)	457		0.037	
	Solid		486		0.035	
C_{12}	CH_2Cl_2	258(1.85×10^4); 314(9.0×10^3)	390		0.0064	
	Water	268; 336	498	162	0.014	98
	Solid		500		0.028	
3-F-C_{12}	CH_2Cl_2	254(2.1×10^4); 314(4.6×10^3); 412(1.2×10^3)	445		0.004	
	Water	268; 380	501	121	0.11	70
	Solid		514		0.091	
3-Cl-C_{12}	CH_2Cl_2	258(3.99×10^4); 322(1.26×10^4); 420(2.0×10^3)	434		0.0045	
	Water	276; 394	502	108	0.44	98
	Solid		519		0.75	
Naph-C_{12}	CH_2Cl_2	306(2.41×10^4); 360(7.6×10^3); 402(1.85×10^3); 422(1.87×10^3)	457		0.037	
	Solid		484		0.044	
4-OH-C_{12}	CH_2Cl_2	275(3.77×10^4); 305(3.66×10^4); 385(7.6×10^3)	409		0.0022	
Cy	CH_2Cl_2	254(2.19×10^4); 316(8.3×10^3)	458		0.067	

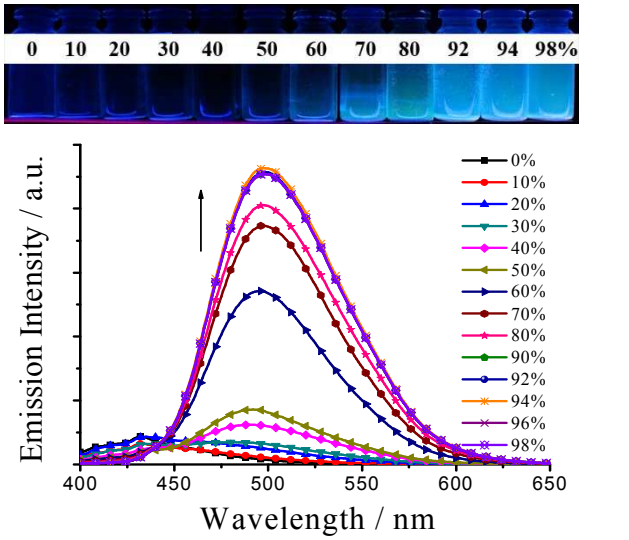

Fig. 4 Emission spectra and photographs (under 360 nm UV light) of $\mathbf{C_2}$ in MeCN–H_2O with different *f* values (1×10^{-5} dm^3 mol^{-1}).

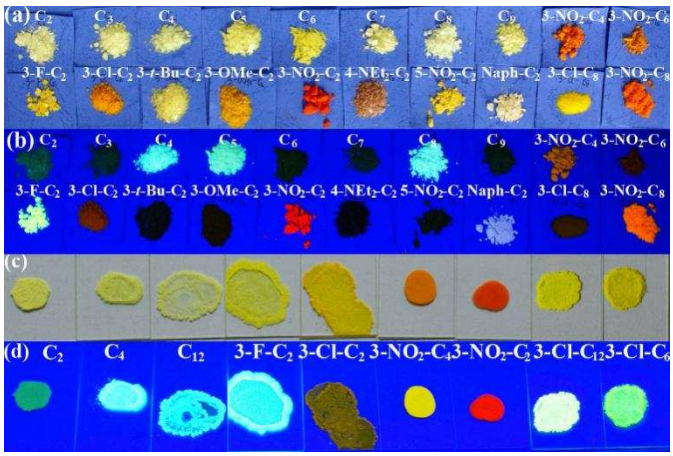

Fig. 5 Photographs (a, c: under room light; b, d: under 360 nm UV light) of some selected Salen ligands in solid state (a, b; $\mathbf{C_6}$ and $\mathbf{C_9}$ are in crystal) and casting films (c, d; CH_2Cl_2 solvent).

The aggregated $\mathbf{C_n}$ (n = 2, 4–6, 8, 9, 12), **3-F-C_n** (n = 2–9, 12), **3-Cl-C_n** (n = 2, 4, 6, 8, 12), **3-NO_2-C_n** (n = 2, 4, 6, 8), **3-OH-C_n** (n = 2, 4), **4-OH-C_n** (n = 2, 4, 6, 8, 12), **5-NO_2-C_4**, **3-OMe-C_4**, **4-OMe-C_4**, **5-OMe-C_4**, and **Naph-C_n** (n = 2–9, 12) have strong emission in solid state or water, but other aggregated Salen ligands are non-emissive (Table 1). Most of AIE-active Salen ligands have similar emission spectra in solid state and water, but solid samples exhibit much stronger emission (Fig. 5 and Table 1), and thus the discussion will be focused on the AIE characteristics of solid samples. Since the molecule arrangements play a key role in AIE, it's not a strange phenomenon that different solid forms of AIE-active materials have different fluorescence properties. For most of AIE-

active Salen ligands, however, the different solid forms, such as crystal, powder, and casting film, have similar emission, except that **C_6** and **C_9** in powder and casting film exhibit much stronger fluorescence than in crystal (see the later discussion).

The length effect of the central *N*-alkyl chain bridges in AIE-active Salen ligands are explored firstly. As depicted in Fig. 6, like their absorption spectra, **C_2**, **C_4**, **C_5**, **C_6**, **C_8**, **C_9**, and **C_{12}** in solid state have similar emission spectra (λ_{em}: 495–500 nm), indicating that the non-conjugated alkyl bridges have little effect on the emission bands of this serial of Salen ligands. However, if different side functional substituents are introduced to **C_2**, different substituents have different effects on the emission bands. Compared with **C_2** (λ_{em} = 500 nm), **Naph-C_2** (λ_{em} = 473 nm) with a π-extended system shows blue-shifted emission, in contrast, **3-F-C_2** (λ_{em} = 513 nm), **3-Cl-C_2**, (λ_{em} = 555 nm), and **3-NO_2-C_2**, (λ_{em} = 588 nm) containing electron-accepting substituents display red-shifted emission (Fig. 8). This substituent effect is a simple and useful tool to achieve red, green, and blue (RGB) emission (Fig. 5 and 7), which was observed in SA-based AIE materials as well.[20]

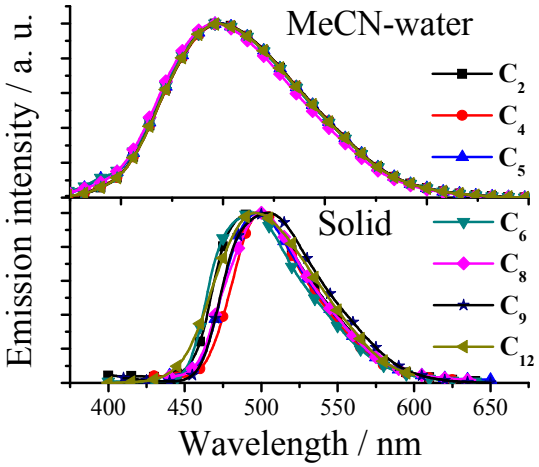

Fig. 6 Normalized emission spectra of **C_n** in MeCN–H_2O (1×10^{-4} dm^3 mol^{-1}, *f* values is listed in Table 1) and solid (**C_6** and **C_9** in powder).

All fluorescence quantum yields (Table 1) of the aggregated Salen ligands in water and solid state were measured by the optical dilute method of Demas and Crosby[23] with a standard of quinine sulfate (Φ_r = 0.55, quinine in 0.05 mol dm^{-3} sulfuric acid) and an integrating sphere, respectively. Although the Salen ligands linking with non-conjugated alkyl bridges have a small π-conjugated system, most of them have unexpected strong fluorescence, as shown in Table 1. In general, the introduction of –F and –Cl would help to achieve AIE with a high fluorescence quantum yield, but the introduction of bulky hindrance substituents of *–t*-butyl and –NEt_2[20d] would bring adversely affects. Since the central *N*-alkyl chain bridges also have an obvious effect on fluorescence quantum yield, –NO_2, –OMe, and naphthalene substituents might influence fluorescence quantum yield positively or negatively. Except **C_5**, Salen ligands **C_n** linking with odd-carbon chain bridges have much weaker AIE than these linking with even-carbon chain bridges. Especially, **3-Cl-C_{12}** has a highest fluorescence quantum yield up to 0.44 and 0.75 in water and solid, respectively. Such chlorination was also found to be an efficient way to improve fluorescence quantum yield in our previous work.[17a,20d]

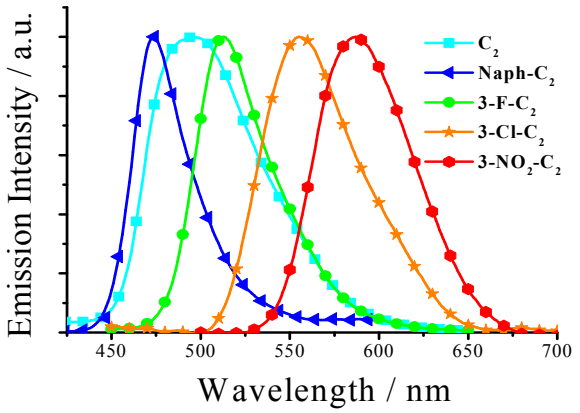

Fig. 7 Normalized emission spectra of **C_2** with different side functional substituents in solid state.

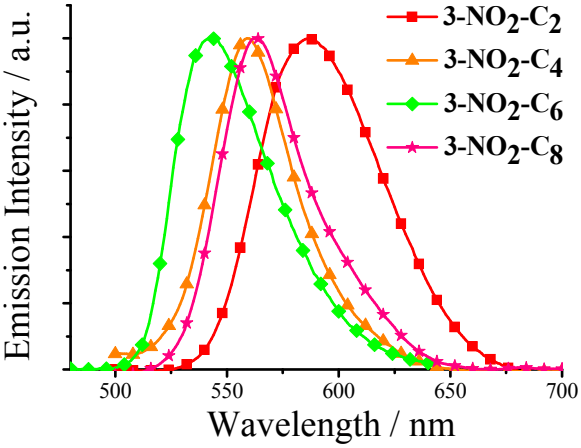

Fig. 8 Normalized emission spectra of **3-NO_2-C_n** in solid state.

Mechanism of AIE

It is interesting that, with similar chemical structures, some of the aggregated Salen ligands are highly emissive, but others are non-emissive. The molecule arrangements play a key role in AIE. For AIE-active materials, slight modification of the chemical structures could alter the molecule arrangements and AIE properties significantly. Non-covalent molecular interactions are frequently involved in the crystallization process to assist the molecules to orient and assemble. In order to achieve a high fluorescence quantum yield, AIE-active dyes should stack closely with a short interplanar distance (for plane molecules, such as SA[20d]) or intermolecular aromatic $H_{Ar}\cdots\pi$ hydrogen bonds (for non-plane molecules, such as TPE or silole[10]) and weak intermolecular face-to-face π–π interactions. The former can ensure to eliminate the molecular rotation, the later would prevent the formation of excimer.[10] For our case, however, the Salen ligands have plane π-conjugated units of iminomethylphenol and non-plane alkyl chain bridges. The

restriction of C–C single bond rotations in the central alkyl chain bridges is another key to achieve AIE, and thus other non-covalent intermolecular interactions, such as N···H, O···H, and H···H, should be considered.

Firstly, in order to investigate the length effect of the central *N*-alkyl chain bridges on molecule arrangements, the x-ray single crystals of $\mathbf{C_2}$, $\mathbf{C_3}$, $\mathbf{C_4}$, $\mathbf{C_5}$, $\mathbf{C_6}$, and $\mathbf{C_9}$ are depicted in Fig. 9. Unlike plane-like SA molecules whose atoms are located in one plane of π-conjugated system,[20d] step-like $\mathbf{C_n}$ molecules have two π-conjugated planes of iminomethylphenol which are separated by the alkyl chain bridges (Fig. 9). It is an interesting phenomenon that the two π-conjugated planes are almost parallel for odd-carbon chain bridges ($\mathbf{C_2}$, $\mathbf{C_4}$, and $\mathbf{C_6}$), nonetheless they are almost vertical for even-carbon chain bridges ($\mathbf{C_3}$, $\mathbf{C_5}$, and $\mathbf{C_9}$).

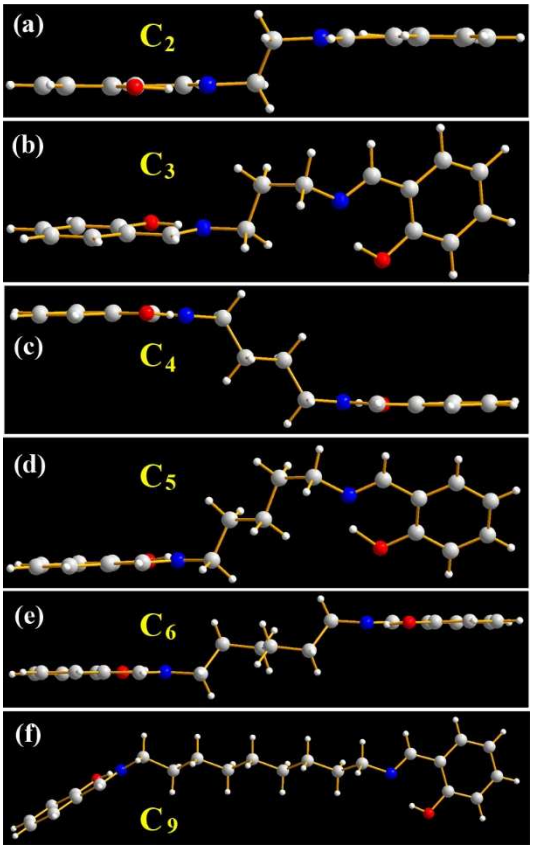

Fig. 9 X-ray single crystal structures of $\mathbf{C_n}$.

As expected, the intramolecular N···H hydrogen bonds (1.673 and 1.787 Å) between H atom in –OH and N atom are found in $\mathbf{C_2}$. Cross-stacking $\mathbf{C_2}$ molecules exhibit an edge-to-face herringbone packing motif (Fig. 10) without any efficient intermolecular face-to-face π–π interactions (overlaps in π-conjugated units, Fig. 10a), which is beneficial to prevent the formation of excimer. On the other hand, many other strong intermolecular interactions including $H_{Ar}\cdots\pi$ hydrogen bonds (2.847 and 3.022 Å), and $H_{OH}\cdots H_{Ak}$ (2.690 Å) (Ak = alkyl), $H_{Ak}\cdots H_{Ak}$ (2.516 Å), and $N\cdots H_{Ak}$ (2.784 Å) interactions are found in the two closest molecules (Fig. 10c). These above intramolecular and intermolecular interactions ensure to eliminate the rotation of N–C and C–C single bonds and result in the presence of AIE thereby.

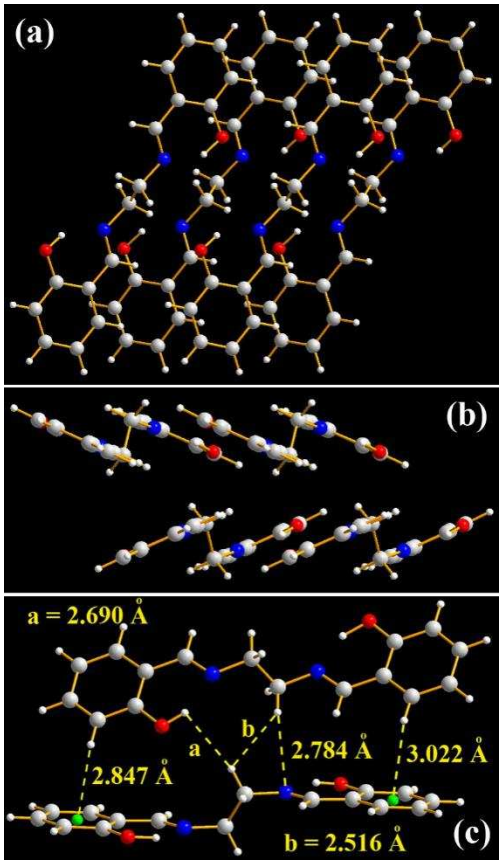

Fig. 10 X-ray single crystal structures and packing of $\mathbf{C_2}$ molecules (a: side view; b: top view; d: intermolecular interactions of the two closest molecules).

Unlike $\mathbf{C_2}$ molecules, $\mathbf{C_3}$ molecules have a very complicated and magic packing (Fig. 11a), even though they have similar chemical structures. There are many strong intermolecular interactions including $H_{Bz}\cdots\pi$ (Bz = benzyl) (2.878 Å) and $H_{Ak}\cdots$ (2.548 and 2.828 Å) interactions in the two closest $\mathbf{C_3}$ molecules (Fig. 11b) as well. On the other hand, $\mathbf{C_3}$ molecules have strong face-to-face π–π interactions (Fig. 11d) with a *d* value of 3.409 Å (Fig. 11c), resulting in the absence of fluorescence.

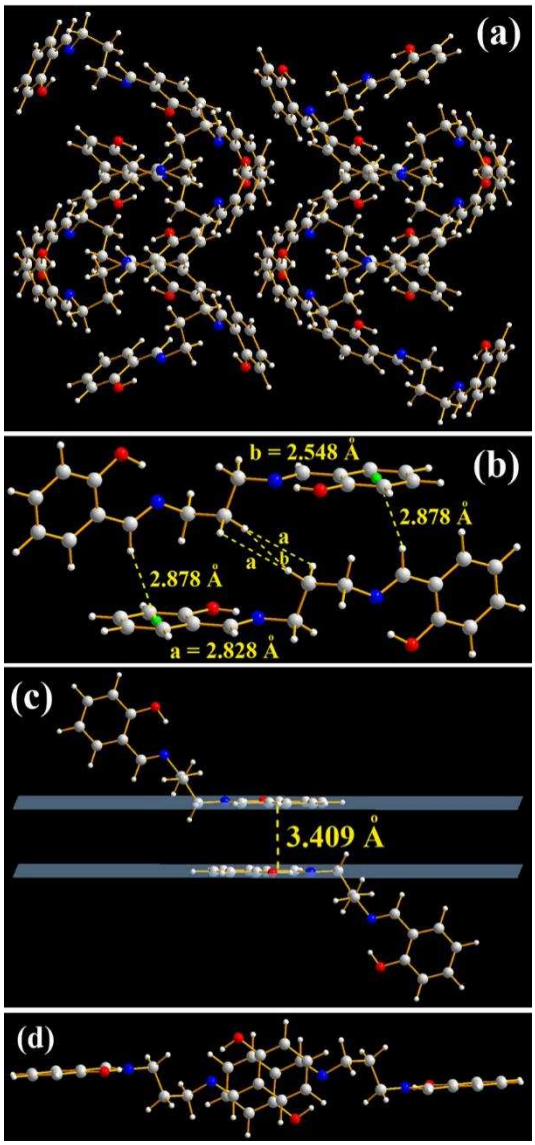

Fig. 11 X-ray single crystal structures and packing of $\mathbf{C_3}$ molecules (a: side view; b: intermolecular interactions of the two closest molecules; c: side view of face-to-face π–π interactions; d: top view of face-to-face π–π interactions).

With a longer length of alkyl chain, $\mathbf{C_4}$ molecules have a uniform packing (Fig. 12a and 12b). Like $\mathbf{C_2}$ molecules, $\mathbf{C_4}$ molecules exhibit a similar edge-to-face herringbone packing with little intermolecular face-to-face π–π interactions (Fig. 12b). Moreover, it should be noted that the intermolecular $H_{Ak}\cdots H_{Ak}$ interaction (2.443 Å) of two neighboring $\mathbf{C_4}$ molecules is stronger than that of $\mathbf{C_2}$ molecules, which might be one possible reason that the aggregated $\mathbf{C_4}$ molecules have a higher fluorescence quantum yield (0.19). $\mathbf{C_5}$ molecules have similar molecular packing and intermolecular interactions (Fig. S7), resulting in the strong AIE like $\mathbf{C_4}$ molecules.

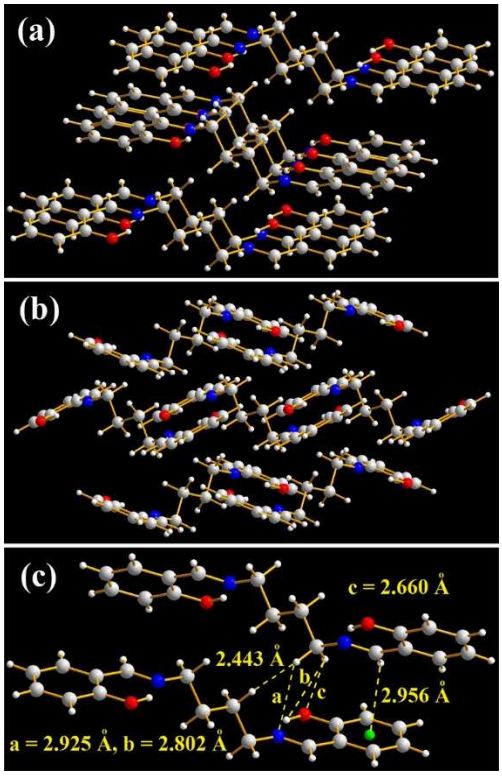

Fig. 12 X-ray single crystal structures and packing of $\mathbf{C_4}$ molecules (a: top view; b: side view; c: intermolecular interactions of the two closest molecules).

Unlike $\mathbf{C_4}$ molecules, $\mathbf{C_6}$ molecules have a cross lamellar packing (Fig. S8). $\mathbf{C_4}$ molecules exhibit an edge-to-face herringbone packing motif without efficient intermolecular face-to-face π–π interactions, but $\mathbf{C_6}$ molecules show a slipped face-to-face lamellar packing with moderate intermolecular face-to-face π–π interactions (d = 3.413 Å, Fig. S8d and S8e). Moreover, the intermolecular interactions (2.738 and 2.794 Å for $H_{Ak}\cdots H_{Ak}$ and $H_{Ar}\cdots H_{Ar}$ interactions, respectively, Fig. S8c) of two neighboring $\mathbf{C_6}$ molecules is a bit weaker than those of $\mathbf{C_4}$ molecules. And thus the single crystals of $\mathbf{C_6}$ are nonemissive.

Since the florescence properties of AIE-active materials are dependent on their molecule arrangements, they have been found to show mechanochromism upon the transition of crystalline and amorphous states under external stimuli.[10] In general, upon applying mechanical force, most of AIE-active materials that own mechanochromic properties exhibit a red shift in emission bands with a decrease in fluorescence intensity. Mechanochromic AIE-active materials showing turn-on fluorescence are still rare.[10,24] Moreover, as the above discussion, the previous works[21] reveal that the presence of side alkyl chains at the AIE-active core would affect the mechanochromic AIE properties, and thus we tried to examine the mechanochromic AIE properties of these Salen ligands. Most of the Salen ligands have no mechanochromic AIE properties. However, it is fortunate to find that $\mathbf{C_6}$ is a mechanochromic material showing turn-on fluorescence. As shown in Fig. 13 and S9, when the pristine crystal solids of $\mathbf{C_6}$ are ground with a spatula, the resulted powders of $\mathbf{C_6}$ have

strong green emission under the irradiation of UV light. The same emission enhancement is also observed if CH_2Cl_2 solution is added to the pristine crystal solids of **C_6** molecules and then the added CH_2Cl_2 solution evaporates fast by reduced pressure distillation. The powders of **C_9** show a similar fluorescence enhancement like **C_6**, but both the powders and crystals of **C_4** emit strong green fluorescence (Fig. 14).

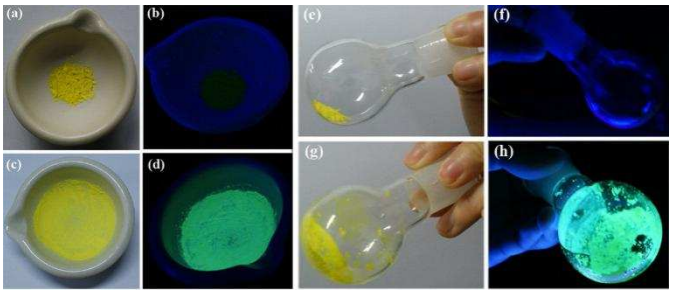

Fig. 13 Photographs of **C_6** solids (a, b, e, f: crystals; c, d: ground solids; g, h: fast evaporated solids) under sunlight or 360 nm UV light.

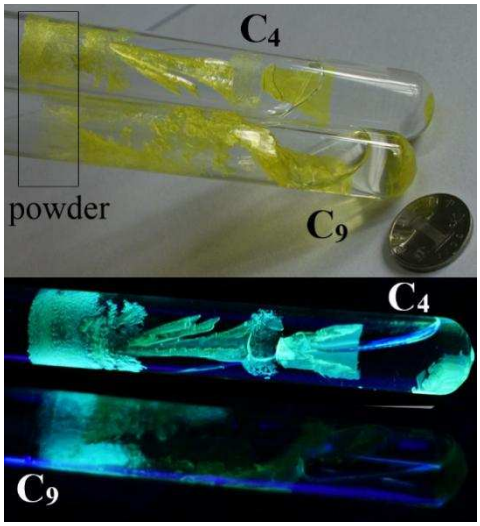

Fig. 14 Photographs of **C_4** and **C_9** solids (the solids at the middle of the tubes are powders, but they are crystals below the middle of the tubes) under sunlight or 360 nm UV light (the diameter of dime is about 2.0 cm).

To gain an insight into the mechanochromic behavior of **C_6** molecules, powder wide-angle X-ray diffraction experiments were conducted on the pristine crystal, ground and evaporated solids. As shown in Fig. 15, all the solid samples show intense and sharp reflection peaks, which are in good agreement with the simulated pattern of single crystal of **C_6**. This indicates that all the solid samples contain microcrystallites and accords with the fact that **C_6** molecules containing a long chain bridge are easy to crystallize (Fig. S9). Most of mechanochromic AIE-active materials process a phase transition from a crystalline to an amorphous phase,[10,21] however, for **C_6** solids, no such phase transition is found. Therefore, the mechanochromic behavior of **C_6** might be responsible for its lamellar packing (Fig. S8a) that is in favor of molecule movement under the external mechanical pressure. If an external mechanical pressure is applied on the crystal, the regular intermolecular face-to-face π–π interactions of **C_6** molecules may be damaged by molecule movement, and thus the fluorescence can be turned on. For the case of fast evaporated solids, the solvent molecules of CH_2Cl_2 may invade into the **C_6** crystal lattice and partially dissolve the crystal. Simultaneously, there is not enough time for the dissolved molecules to stack closely and regularly by π–π interactions during fast CH_2Cl_2 evaporation, leading to the formation of crystal defects at the etched area. Such crystal-defect-induced emission was also observed in a diaminomaleonitrile-based Schiff base.[24]

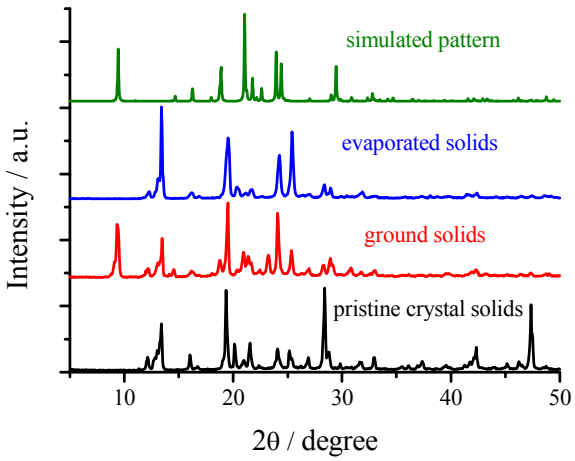

Fig. 15 X-ray powder diffraction of **C_6** solids.

Owing to the similar lamellar packing (Fig. S10), the single crystals of **C_9** also show a very lower fluorescence quantum yield like the single crystals of **C_6** (Fig. S8). It is worth noting that **C_9** molecules containing the second longest chain can self-assemble to build very beautiful and wonderful molecular constructions, such as batman (Fig. S10b) and luxuriant palace lantern (Fig. S10c), and big single crystals (Fig. 14), which might have some potential applications in molecular self-assembly.

Next, the x-ray single crystal structures of **3-OMe-C_2** and **3-F-C_2** are discussed to investigate the substituent effect on molecule arrangements. Our previous work[20d] demonstrated that the presence of different electron-accepting and electron-donating substituents at SA molecule is an efficient way to tune molecular packing and AIE properties thereby. As shown in Fig. S11a, **3-OMe-C_2** molecules exhibit a brick-wall packing that provides two-dimensional percolation paths for strong face-to-face π–π interactions (d = 3.310 Å, Fig. S11b and S11c) and lead to the absence of AIE consequently.

However, if –OMe substituents are taken placed by –F substituents, **3-F-C_2** molecules have a totally different packing from **3-OMe-C_2** molecules in spite of the fact that there is no any strong halogen bond (Fig. 16). As shown in Fig. 16a and 16b, **3-F-C_2** molecules exhibit a very uniform edge-to-face herringbone packing like **C_2** molecules, resulting in the formation of big single crystals (~2.0 cm, Fig. 16c) conveniently. There are no face-to-face π–π interactions but many other strong intermolecular interactions in two neighboring **3-F-**

C_2 molecules. The strongest $H_{OH}\cdots H_{Ak}$ interaction of **3-F-C_2** molecules is 2.465 Å, which is close to the $H_{Ak}\cdots H_{Ak}$ interaction (2.443 Å) of C_4 molecules. And thus, the aggregated **3-F-C_2** molecules have strong AIE like C_4 molecules.

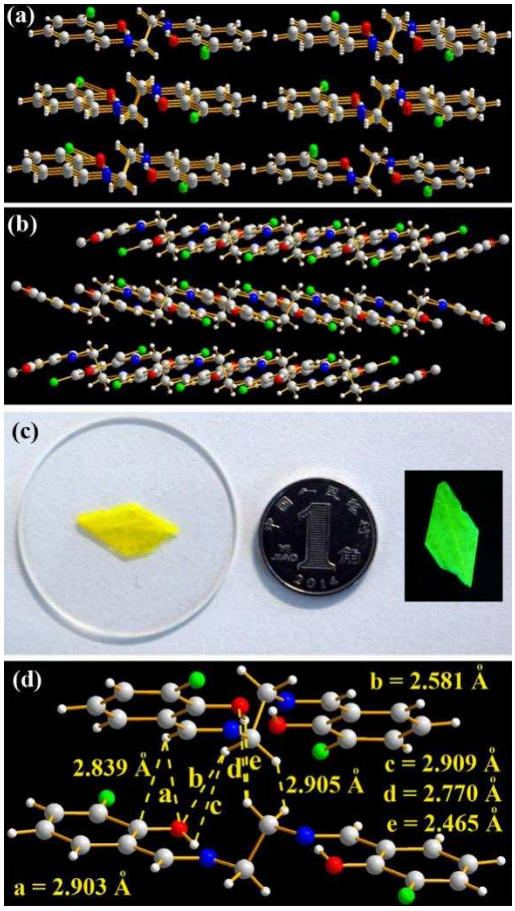

Fig. 16 X-ray single crystal structures and packing of **3-F-C_2** molecules (a: side view; b: side view; c: photographs of the single crystal under sunlight and under 360 nm UV light; d: intermolecular interactions of the two closest molecules; the diameter of dime is about 2.0 cm).

Then, the x-ray single crystal structures of **Cy** are studied to investigate the different effects on molecule arrangements between cycloalkane and *N*-alkane bridges. As shown in Fig. S12, unlike C_n molecules with *N*-alkane bridges, **Cy** molecules with a cyclohexane bridge are not step-like but V-shaped. The two π-conjugated planes of iminomethylphenol in one **Cy** molecule face to each other obliquely, indicting the possible existence of intramolecular π–π interactions. Moreover, the cyclohexane bridges in the neighboring V-shaped **Cy** molecules are separated without any strong intermolecular interactions (> 4 Å). Therefore, the aggregated **Cy** molecules have no AIE.

Finally, for the purpose of the mechanism evaluation, the photophysical properties of reference substances, **Ref1**, **Ref2**, **Ref3,** and **Ref4**, were tested. Like the Salen ligands, **Ref1** and **Ref2** are *bis*-Schiff bases, and thus they are solid at room temperature. Conversely, mono-Schiff bases **Ref3** and **Ref4** are oil. All of them (solid or oil samples) are nonemissive at room temperature, indicating that both *bis*-Schiff base structure and –OH groups of Salen ligands are of greatest importance for AIE. *Bis*-Schiff base structure presumably enables strong intermolecular interactions between π-conjugated iminomethylphenol groups in the two closest molecules (Fig. 10c, 12c, S7c, S8c, and 16d) to achieve AIE. Through the intramolecular hydrogen bonds, the –OH groups can efficiently prevent two phenolic rings from IRs and non-radiative annihilations. Additionally, these intramolecular hydrogen bonds would lead to keto and enol tautomers through an ultrafast excited-state intramolecular-proton transfer (ESIPT) process.[20d] The AIE-active dyes with ESIPT offer some additional advantages, such as a large Stokes shift with a low background signal from the excitation light source. These large Stokes shifts combining with the facts of small π-conjugated systems but highly emissive solids enabled us to wonder whether the emission of these Salen ligands originated from fluorescence, because recently some reports[25] demonstrated that some pure organic compounds containing small π-conjugated systems show strong solid-state phosphorescence at room temperature. However, time-resolved emission spectra (Fig. S13) reveal that the emission decay lifetime of C_4, **3-F-C_2**, and **3-Cl-C_{12}** (powder) is 1.7, 3.3, and 5.5 ns, respectively. This confirms the fact that their emission originates from fluorescence rather than phosphorescence. The tendency in emission decay lifetime (C_4 < **3-F-C_2** < **3-Cl-C_{12}**) is consistent with that in fluorescence quantum yield (Φ = 0.19, 0.38, and 0.75 for C_4, **3-F-C_2**, and **3-Cl-C_{12}**, respectively).

Living cell imaging

Fluorescent dyes are promising tools for turn-on, real-time, on-site and non-invasive visualization of biological molecules and processes in live cells and organisms. Furthermore, AIE-active dyes offer higher resistance to photobleaching and thus superior photostability and higher signal reliability relative to conventional dyes.[26] For a useful fluorescent biological tracer, it should neither inhibit nor promote the growth of living cells. The HeLa cells were imaged by the Salen ligands using a standard cell-staining protocol. The living cells were incubated with the Salen ligands for 2 h and then washed three times with phosphate buffered saline (PBS) solution. As can be seen from Fig. 17, incubated with **Naph-C_2**, C_4, **3-F-C_2**, **3-F-C_8**, **3-Cl-C_{12}**, and **3-NO_2-C_8**, the HeLa cells grow similar as in the control experiments in the absence of the dyes, indicating that the Salen ligands exert less toxicity on the living cells. HeLa cells show negligible background fluorescence (Fig. 17b). However, after incubation with the Salen ligands, intense intracellular blue, green, yellow, or red fluorescence with high signal-to-noise ratio is observed (Fig. 17c–d). Some commercially available fluorescence dyes, such as CellTracker Green, stain the entire cells, and only the cytoplasmic regions of the cells are stained by TPE- or silole-based dyes.[27] It is interesting that the Salen ligands, especially for **3-Cl-C_{12}** (Fig. 17f) and **3-NO_2-C_8** (Fig. 17g), mainly stain the nucleus of living HeLa cells. The colorful AIE-active Salen ligands may thus be used to probe or monitor biologically important processes in vitro as well as in vivo.

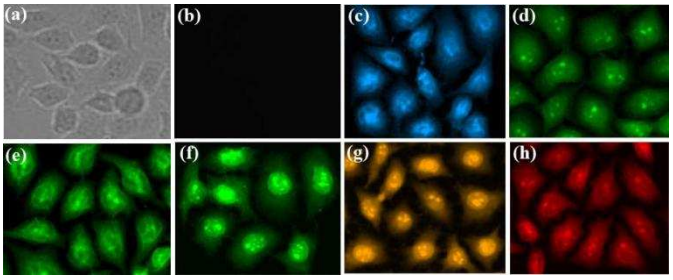

Fig. 17 Brightfield (a, incubated without dye) and fluorescence images (b, incubated without dye; c, incubated with **Naph-C_2**; d, incubated with **C_4**; e, incubated with **3-F-C_2**; e, incubated with **3-F-C_8;** f, incubated with **3-Cl-C_{12};** g, incubated with **3-NO_2-C_8;** h, incubated with **3-NO_2-C_2**) of HeLa cells.

Conclusion

We have systematically synthesized and studied the unique AIE properties, mechanofluorochromism, and cell imaging applications of a series of Salen Schiff Bases. The chemical structures of these Salen ligands have a significant influence on their molecule arrangements and consequently AIE properties. Both weak intermolecular face-to-face π–π interactions and strong non-covalent intermolecular interactions such as N···H, O···H, H···H, and H···π are the key factors to achieve AIE. Although these Salen ligands linking with non-conjugated alkyl bridges have a small π-conjugated system, they show strong red, green, and blue AIE. The fluorescence colors can be well-tuned by the introduction of side functional substituents, π-extended system, or central *N*-alkyl chain bridges. The introduction of electron-accepting substituents of $–NO_2$, –F, and –Cl and π-extended system of naphthalene ring would help to induce red- and blue-shifted emission respectively. Especially, combining with the help of side functional substituents, the central non-conjugated alkyl bridges have a much obvious effect on tuning fluorescence bands. Moreover, it has been revealed that chlorination and fluorination are an efficient way to achieve high fluorescence quantum yield. Therefore, we believe that these simple Salen ligands provide a new paradigm in the design of AIE-active dyes for developing advanced organic optoelectronic devices, florescent probes, and cell imaging, and so on.

Acknowledgements

This work was supported by the National Natural Science Foundation of China (no. 21172160, 21272161, and 21372169).

Notes and references

[a] *College of Chemistry, Sichuan University, Chengdu, 610041, China. Fax: (+86) 28-8541-2291. E-mail: xianghaifeng@scu.edu.cn.*

[b] *Laboratory of Stem Cell Biology, State Key Laboratory of Biotherapy, West China Hospital, Sichuan University, Chengdu, 610064, China. E-mail: ljamelia@163.com.*

† Electronic Supplementary Information (ESI) available: General, materials, computational details, crystallographic information files (CIF), crystallographic data, absorption, emission data, SEM, DLS, TGA, DSC, and IR spectra. CCDC 1417706 (**C_4**), 1417707 (**3-F-C_2**), 1417708 (**C_6**), 1417709 (**C_5**), and 1417710 (**C_9**). See DOI: 10.1039/b000000x/

‡ These authors contributed equally to this work.

1 B. Valeur, *Molecular Fluorescence: Principles and Applications*, Wiley, 2002.

2 (a) U. Mitschke and P. Bauerle, *J. Mater. Chem.,* 2000, *10*, 1471; (b) L.S. Hung and C. H. Chen, *Mater. Sci. Eng. R,* 2002, *39*, 143; (c) K. Mullen and U. Scherf, *Organic Light Emitting Devices–Synthesis, Properties and Applications*, Wiley, 2006; (d) Yersin H.; ed. *Highly Efficient OLEDs with Phosphorescent Materials*, Wiley, 2007; (e) H. F. Xiang, J. H. Cheng, X. F. Ma , X. G. Zhou and J. Chruma, J. *Chem. Soc. Rev.,* 2013, *42*, 6128.

3 (a) J. D. Slinker, J. Rivnay, J. S. Moskowitz, J. B. Parker, S. Bernhard, H. D. Abruoac and G. Malliaras, *J. Mater. Chem.,* 2007, *17*, 2976; (b) R. D. Costa, E. Orti and H. J. Bolink, *Pure Appl. Chem.,* 2011, *83*, 2115.

4 (a) T. N. Singh-Rachford and F. N. Castellano, *Coord. Chem. Rev.,* 2010, *254*, 2560; (b) J. Z. Zhao, S. M. Ji and H. M. Guo, *RSC Adv.,* 2011, *1*, 937; (c) J. Z. Zhao, W. H. Wu, J. F. Sun and S. Guo, Chem. *Soc. Rev.,* 2013, *42*, 5323.

5 (a) R. Martinez-Manez and F. Sancenon, *Chem. Rev.,* 2003, *103*, 4419; (b) E. M. Nolan and S. J. Lippard, *Chem. Rev.,* 2008, *108*, 3443; (c) H. N. Kim, M. H. Lee, H. J. Kim, J. S. Kim and J. Yoon, *Chem. Soc. Rev.,* 2008, *37*, 1465; (d) Q. Zhao, F. Y. Li and C. H. Huang, *Chem. Soc. Rev.,* 2010, *39*, 3007; (e) J. F. Zhang, Y. Zhou, J. Yoon and J. S. Kim, *Chem. Soc. Rev*., 2011, *40*, 3416; (f) K. Kaur, R. Saini, A. Kumar, V. Luxami, N. Kaur and P. Singh, *Coord. Chem. Rev*., 2012, *256*, 1992; (g) Y. Feng, J. H. Cheng, L. Zhou, X. G. Zhou and H. F. Xiang, *Analyst,* 2012, *137*, 4885; (h) Y. M. Yang, Q. Zhao, W. Feng and F. Y. Li, *Chem. Rev.*, 2013, *113*, 192; (i) J. H. Cheng, X. G. Zhou and H. F. Xiang, *Analyst*, 2015, DOI: 10.1039/C5AN01398D.

6 (a) R. W. Y. Sun and C. M. Che, *Coord. Chem. Rev*., 2009, *253*, 1682; (b) L. H. Feng, C. L. Zhu, H. X. Yuan, L. B. Liu, F. T. Lv and S. Wang, *Chem. Soc. Rev*., 2013, *42*, 6620.

7 (a) V. Fernandez-Moreira, F. L. Thorp-Greenwood and M. P. Coogan, *Chem. Commun.*, 2010, *46*, 186; (b) Q. Zhao, C. H. Huang and F. Y. Li, *Chem. Soc. Rev*., 2011, *40*, 2508.

8 J. B. Birks, *Photophysics of Aromatic Molecules*, Wiley, 1970.

9 J. Luo, Z. Xie, J. W. Y. Lam, L. Cheng, H. Chen, C. Qiu, H. S. Kwok, X. Zhan, Y. Liu, D. Zhu and B. Z. Tang, *Chem. Commun*., 2001, 1740.

10 (a) Y. Hong, J. W. Y. Lam and B. Z. Tang, *Chem. Commun*., 2009, 4332; (b) M.Wang, G. X. Zhang, D. Q. Zhang, D. B. Zhu and B. Z.Tang, *J. Mater. Chem*., 2010, *20*, 1858; (c) Y. Hong, J. W. Y. Lam and B. Z. Tang, *Chem. Soc. Rev*., 2011, *40*, 5361; (d) A. Qin and B. Z. Tang, *Aggregation-Induced Emission: Fundamentals*, Wiley, 2014.

11 (a) L. Canali and D. C. Sherrington, *Chem. Soc. Rev.,* 1999, *28*, 85; (b) D. A. Atwood and M. J. Harvey, *Chem. Rev*., 2001, *101*, 37; (c) P. G. Cozzi, *Chem. Soc. Rev*., 2004, *33*, 410.

12 (a) E. Lamour, S. Routier, J. L. Bernier, J. P. Catteau, C. Bailly and H. Vezin, *J. Am. Chem. Soc.,* 1999, *121*, 1862; (b) P. Wu, D. L. Ma, C. H. Leung, S. C. Yan, N. Y. Zhu, R. Abagyan and C. M. Che, *Chem. Eur. J*., 2009, *15*, 13008.

13 (a) P. G. Lacroix, *Eur. J. Inorg. Chem*., 2001, 339; (b) E. Hadjoudis and I. M. Mavridis, *Chem. Soc. Rev*., 2004, *33*, 579; (c) H. Miyasaka, A. Saitoh and S. Abe, *Coord. Chem. Rev*., 2007, *251*, 2622; (d) M. Andruh, *Chem. Commun*., 2011, *47*, 3025.

14 (a) A. W. Kleij, *Dalton Trans*., 2009, 4635; (b) G. Consiglio, S. Failla, I. P. Oliveri, R. Purrello and S. Di Bella, *Dalton Trans*., 2009, 10426; (c) S. J. Wezenberg, E. C. Escudero-Adán, J. Benet-Buchholz and A. W. Kleij, *Chem. Eur. J*., 2009, *15*, 5695; (d) G. Consiglio, S. Failla, P. Finocchiaro, I. P. Oliveri, R. Purrello and S. Di Bella, *Inorg. Chem*., 2010, *49*, 5134; (e) G. Consiglio, S. Failla, P. Finocchiaro, I. P. Oliveri and S. Di Bella, *Dalton Trans*., 2012, *41*, 387.

15 (a) Y. Hai, J. J. Chen, P. Zhao, H. Lv, Y. Yu, P. Y. Xu and J. L. Zhang, *Chem. Commun*., 2011, *47,* 2435; (b) J. Jing, J. J. Chen, Y. Hai, J. H. Zhan, P. Y. Xu and J. L. Zhang, *Chem. Sci*., 2012, *3*, 3315; (c) J. Jing and J. L. Zhang, *Chem. Sci*., 2013, *4*, 2947; (d) I. Giannicchi, R. Brissos, D. Ramos, J. de Lapuente and J. C. Lima, *Inorg. Chem*., 2013, *52*, 9245; (e) D. Xie, J. Jing, Y. B. Cai, J. Tang, J. J. Chen and J. L. Zhang, *Chem. Sci.*, 2014, *5*, 2318; (f) J. Tang, Y. B. Cai, J. Jing and J. L. Zhang, *Chem. Sci.*, 2015, *6*, 2389.

16 (a) P. F. Wang, Z. R. Hong, Z. Y. Xie, S. W. Tong, O. Y. Wong, C. S. Lee, N. B. Wong, L. S. Hung and S. T. Lee, *Chem. Commun*., 2003, 1664; (b) C. M. Che, S. C. Chan, H. F. Xiang, M. C. W. Chan, Y. Liu and Y. Wang, *Chem. Commun*., 2004, 1484; (c) H. F. Xiang, S. C. Chan, K. K. Y. Wu, C. M. Che and P. T.Lai, *Chem. Commun*., 2005, 1408; (d) J. O. Huh, M. H. Lee, H. Jang, K. Y. Hwang, J. S. Lee, S. H. Kim and Y. Do, *Inorg. Chem*., 2008, *47*, 6566; (e) K. Y. Hwang, H. Kim, Y. S. Lee, M. H. Lee and Y.Do, *Chem. Eur. J*., 2009, *15*, 6478; (f) Y. Zhou, J. W. Kim, R. Nandhakumar, M. J. Kim, E. Cho, Y. S. Kim, Y. H. Jang, C. Lee, S. Han, K. M. Kim, J. J. Kim and J.Yoon, *Chem. Commun*., 2010, *46*, 6512; (g) C. M. Che, C. C. Kwok, S. W. Lai, A. F. Rausch, W. J. Finkenzeller, N. Y. Zhu and H. Yersin, *Chem. Eur. J*., 2010, *16*, 233; (h) J. Zhang, F. C. Zhao, X. J. Zhu, W. K. Wong, D. G. Ma and W. Y. Wong, *J. Mater. Chem*., 2012, *22*, 16448.

17 (a) L. Zhou, P. Y. Cai, Y. Feng, J. H. Cheng, H. F. Xiang, J. Liu, D. Wu and X. G. Zhou, *Anal. Chim. Acta,* 2012, *735*, 96; (b) L. Zhou, Y. Feng, J. H. Cheng, N. Sun, X. G. Zhou and H. F.Xiang, *RSC Adv*., 2012, *2*, 10529; (c) J. H. Cheng, K. Y. Wei, X. F. Ma, X. G. Zhou and H. F. Xiang, *J. Phys. Chem. C,* 2013, *117*, 16552; (d) J. H.Cheng, Y. H. Zhang, X. F. Ma, X. G. Zhou and H. F. Xiang, *Chem. Commun*., 2013, *49*, 11791; (e) J. H. Cheng, X. F. Ma, Y. H. Zhang, J. Y. Liu, X. G. Zhou and H. F. Xiang, *Inorg. Chem*., 2014, *53*, 3210.

18 (a) J. Wang, J. Mei, R. Hu, J. Z. Sun, A. Qin and B. Z. Tang, *J. Am. Chem. Soc*., 2012, *134*, 9956; (b) C. W. T. Leung, Y. Hong, S. Chen, E. Zhao, J. W. Y. Lam and B. Z. Tang, *J. Am. Chem. Soc*., 2013, *135*, 62; (c) S. Chen, Y. Hong, Y. Liu, J. Liu, C. W. T. Leung, M. Li, R. T. K. Kwok, E. Zhao, J. W. Y. Lam, Y. Yu and B. Z. Tang, *J. Am. Chem. Soc*., 2013, *135*, 4926; (d) Z. Wang, S. Chen, J. W. Y. Lam, W. Qin, R. T. K. Kwok, N. Xie, Q. Hu and B. Z.Tang, *J. Am. Chem. Soc*., 2013, *135*, 8238.

19 (a) Y. Liu, Y. Tang, N. N. Barashkov, I. S. Irgibaeva, J. W. Y. Lam, R. Hu, D. Birimzhanova, Y. Yu and B. Z.Tang, *J. Am. Chem. Soc*., 2010, *132*, 13951; (b) Y. Yuan, R. T. K. Kwok, B. Z. Tang and B. Liu, *J. Am. Chem. Soc*., 2014, *136*, 2546.

20 (a) W. Tang, Y. Xiang and A. Tong, *J. Org. Chem*., 2009, *74*, 2163; (b) R. Wei, P. Song and A. Tong, *J. Phys. Chem. C,* 2013, *117*, 3467; (c) X. Chen and A.Tong, *J. Lumin*., 2014, *145*, 737; (d) X. F. Ma, J. H. Cheng, J. Y. Liu, X. G. Zhou and H. F. Xiang, *New J. Chem*., 2015, *39*, 492.

21 (a) M. Zheng, M. Sun, Y. Li, J. Wang, L. Bu, S. Xue and W. Yang, *Dyes Pigment*, 2014, *102*, 29; (b) P. Xue, B. Yao, X. Liu, J. Sun, P. Gong, Z. Zhang, C. Qian, Y. Zhang and R. Lu, *J. Mater. Chem. C,* 2015, *3*, 1018.

22 (a) H. F. Xiang, S. C. Yu, C. M. Che and P. T. Lai, *Appl. Phys. Lett*., 2003, *83*, 1518; (b) C. M. Che, H. F. Xiang, S. S. Y. Chui, Z. X. Xu, V. A. L. Roy, J. J. Yan, W. F. Fu, P. T. Lai and I. D. Williams, *Chem. Asian J*., 2008, *3*, 1092; (c) Z. X. Xu, H. F. Xiang, V. A. L. Roy, S. S. Y. Chui, C. M. Che and P. T. Lai, *Appl. Phys. Lett*., 2008, *93*, 223305; (d) H. F. Xiang, L. Zhou, Y. Feng, J. H. Cheng, D. Wu and X. G. Zhou, *Inorg. Chem*., 2012, *51*, 5208; (e) L. Zhou, Z. X. Xu, Y. Zhou, Y. Feng, X. G. Zhou, H. F. Xiang and V. A. L. Roy, *Chem. Commun*., 2012, *48*, 5139.

23 J. N. Demas and G. A. Crosby, *J. Phys. Chem.,* 1971, *75*, 991.

24 T. Han, Y. Hong, N. Xie, S. Chen, N. Zhao, E. Zhao, J. W. Y. Lam, H. H. Y. Sung, Y. Dong, B. Tong and B. Z. Tang, *J. Mater. Chem. C,* 2013, *1*, 7314.

25 S. Mukherjee and P. Thilagar, *Chem. Commun*., 2015, *51*, 10988.

26 J. Liang, B. Z. Tang and B. Liu, *Chem. Soc. Rev*., 2015, *44*, 2798.

27 (a) Y. Hong, H. Xiong, J. W. Y. J Lam, M. Haußler, J. Liu, Y. Yu, Y. Zhong, H. H. Y. Sung, I. D. Williams, K. S. Wong and B. Z.Tang, *Chem. Eur. J*., 2010, *16*, 1232; (b) M. Faisal, Y. Hong, J. Liu, Y. Yu, J. W. Y. Lam, A. Qin, P. Lu and B. Z. Tang, *Chem. Eur. J*., 2010, *16*, 4266.

Functionalized Salen ligands linking with non-conjugated bridges: unique and colorful aggregation-induced emission, mechanism, and applications

Jinghui Cheng, Yuanxi Li, Rui Sun, Jiaoyan Liu, Fei Gou, Xiangge Zhou, Haifeng Xiang, and Jin Liu

Graphical abstract

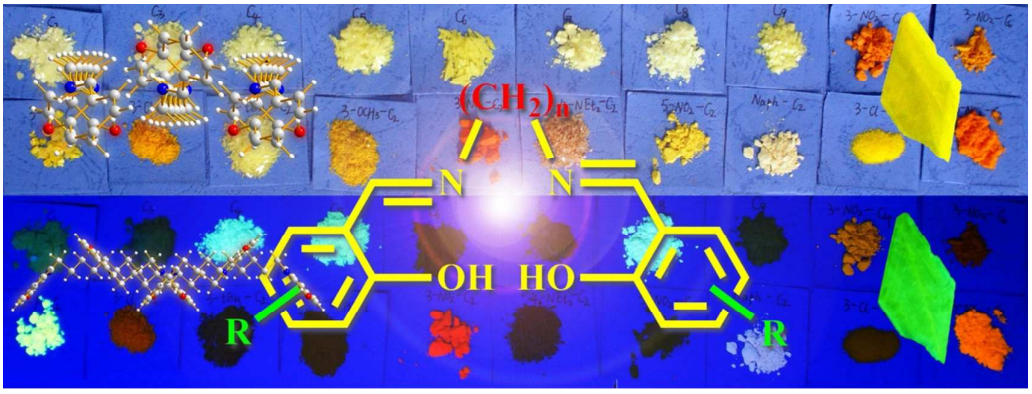

A series of novel, simple, and useful Salen ligands (56 samples) linking with different non-conjugated alkyl bridges have a small π-conjugated system but exhibit strong red, green, and blue AIE.